Transport through artificial single-molecule magnets: Spin-pair state sequential tunneling and Kondo effects*

Niu Peng-Bin(牛鹏斌), Wang Qiang(王 强), and Nie Yi-Hang(聂一行)†

Institute of Theoretical Physics and Department of Physics, Shanxi University, Taiyuan 030006, *China*

(Received 30 May 2012; revised manuscript received 31 August 2012)

The transport properties of an artificial single-molecule magnet based on a CdTe quantum dot doped with a single Mn^{+2} ion ($S = 5/2$) are investigated by the non-equilibrium Green function method. We consider a minimal model where the Mn–hole exchange coupling is strongly anisotropic so that spin-flip is suppressed and the impurity spin S and a hole spin s entering the quantum dot are coupled into spin pair states with $(2S+1)$ sublevels. In the sequential tunneling regime, the differential conductance exhibits $(2S+1)$ possible peaks, corresponding to resonance tunneling via $(2S+1)$ sublevels. At low temperature, Kondo physics dominates transport and $(2S+1)$ Kondo peaks occur in the local density of states and conductance. These peaks originate from the spin-singlet state formed by the holes in the leads and on the dot via higher-order processes and are related to the parallel and antiparallel spin pair states.

Keywords: artificial single-molecule magnet, Hubbard Green function, spin-pair Kondo effect

PACS: 73.63.Kv, 72.10.–d, 72.15.Qm, 73.63.–b **DOI:** 10.1088/1674-1056/22/2/027307

1. Introduction

Single-molecule magnets (SMMs) such as Mn_{12} or Fe_8 have attracted much attention in the last two decades for showing the macroscopic quantum coherence and macroscopic quantum tunneling.[1,2] Since Heersche *et al*. trapped an SMM in a typical field-effect transistor geometry,[3] great efforts have been made to investigate the electron transport through an SMM due to its potential applications and pure scientific interests.[4–6] The realization of the magnetic single-molecule transistor confirms the feasibility of the combination of the molecular electronics and spintronics.[3,6] In particular, theoretical and experimental studies on SMM quantum transport have exhibited a lot of fascinating transport properties such as negative differential conductance,[3,7] the Kondo effect,[4,5,8–10] current-induced switching,[11–13] Berry phase blockade and oscillations,[1,14] graphene spintronics,[15,16] shot noise,[17–20] and so on. Although the single molecule magnets like Mn_{12} have been trapped in a three-terminal transport setup and the electron transport through a single-molecule transistor can be probed,[3,6] the properties of the setup are dependent on the single molecule magnet and can hardly be tuned once it is fabricated.[21] Thus one thinks of the artificial counterparts to molecules,[22–24] such as SMM. The successful fabrication of quantum dot (QD)[25–33] doped with a single Mn^{+2} ion has stimulated many studies on the quantum dot with a single magnetic ion. The theoretical investigation indicates that a II–VI semiconductor QD doped with a single Mn atom behaves like a tunable nanomagnet whose magnetization and anisotropy can be manipulated electrically.[21] Recently, Mn-doped QD, such as a CdTe QD doped with a single Mn^{+2} ion with spin $S = 5/2$, is proposed as an artificial single-molecule magnet (ASMM).[34] The rich physics of the artificial single-molecule magnets is reflected in the transport properties through the system.[34] Hence it is expected that the artificial single-molecule magnets may be useful for improving the controllability of the molecular spintronics devices.

In this paper we study the transport properties of an ASMM in the sequential and Kondo regimes. In the transport setup the Mn–hole exchange interaction is strongly anisotropic so that the spin-flip is suppressed. As a result the impurity spin state and a hole spin state are coupled into spin pair states with $(2S+1)$ sublevels (S is impurity spin), which leads to the conductance depending on the quantum state of the Mn spin and not uniquely determined by the gate and the bias voltage. In the sequential tunneling regime, $(2S+1)$ peaks occur in the differential conductance spectrum, corresponding to resonance tunneling via $(2S+1)$ sublevels. At low temperature, Kondo physics dominates transport. The differential conductance and local density of states (DOS) exhibit $(2S+1)$ Kondo peaks, which is different from the Kondo effects in the molecular magnet induced by the quantum tunneling of the moment[4,5] and also differs from Kondo effects in a half-integer-spin[35] or an integer-spin QD.[36] It originates from the exchange interaction between the hole spin and the impurity spin in ASMM. The exchange interaction splits the initial singly-occupied level into $(2S+1)$ sublevels. The holes in the leads and on the sublevel form a spin-singlet state via higher-order processes, which leads to the Kondo effects depending on the parallel and antiparallel spin pair states.

*Project supported by the National Natural Science Foundation of China (Grant Nos. 10974124 and 11004124) and the Natural Science Foundation of Shanxi Province of China (Grant No. 2009011001-1).

†Corresponding author. E-mail: nieyh@sxu.edu.cn

© 2013 Chinese Physical Society and IOP Publishing Ltd

2. Model of quantum dot with a magnetic impurity

The transport setup considered here consists of a CdTe QD doped with a single Mn^{+2} ion ($S = 5/2$) and two metallic leads coupled to the QD. The full Hamiltonian for the model reads $H = H_{\rm leads} + H_{\rm T} + H_{\rm cen}$. The first term describes the hole reservoir in leads with $H_{\rm leads} = \sum_{k\alpha\sigma} \epsilon_{k\alpha} c^{\dagger}_{k\alpha\sigma} c_{k\alpha\sigma}$. The second term $H_{\rm T} = \sum_{k\alpha\sigma}(t_{k\alpha} c^{\dagger}_{k\alpha\sigma} c_{\sigma} + {\rm H.c.})$ describes tunneling between the leads and the QD with $c^{\dagger}_{\sigma}$ (c_{σ}) creating (destroying) a hole in the QD. The third term is the center Hamiltonian given by[34]

$$\begin{aligned} H_{\rm cen} &= \sum_{\sigma=\uparrow,\downarrow} \epsilon_{\rm h} c^{\dagger}_{\sigma} c_{\sigma} + U n_{\uparrow} n_{\downarrow} + J s_z S_z \\ &\quad + \frac{\gamma J}{2}\left(s_+ S_- + s_- S_+\right). \end{aligned} \tag{1}$$

Here U is the Coulomb repulsion energy on the dot and $n_{\sigma} = c^{\dagger}_{\sigma} c_{\sigma}$ ($\sigma = \uparrow, \downarrow$). $S_{z,\pm}$ are the Mn spin operators and $s_{z,\pm}$ are Pauli matrices acting on the hole lowest energy doublet. The third and the fourth terms describe the effective Mn–hole exchange coupling where γ is a dimensionless parameter depending on the heavy-light hole mixing.[27] The exchange interaction is highly anisotropic due to strong spin–orbit coupling so that the spin-flip between hole and large spin is suppressed ($\gamma = 0$) and we may only consider this special case in the present work. Unless explicitly stated otherwise, we shall henceforth work in units where $e = \hbar = 1$.

In the strong Coulomb blockade limit, the eigenstates of center Hamiltonian $H_{\rm cen}$ have three branches denoted by many-body states $|\lambda, m\rangle = |\lambda\rangle|m\rangle$, where m is the local magnetic quantum number of the Z-component of Mn spin. $\lambda = 0, \uparrow$, and $\downarrow$ denotes the state with no hole, a spin-up hole, and a spin-down hole, respectively. These states satisfy

$$H_{\rm cen}|\lambda, m\rangle = E_{\lambda m}|\lambda, m\rangle, \tag{2}$$

where $E_{0,m} = 0$, $E_{\sigma,m} = \epsilon_{\rm h} + \delta_{\sigma}\frac{J}{2}m$ with $\delta_{\sigma} = +1(-1)$ for $\sigma = \uparrow$ ($\downarrow$) and $E_{\uparrow,m} = E_{\downarrow,-m}$.

Now we rewrite the Hamiltonian in the many-body state representation. First, for strong interaction ($U \to \infty$), we can rewrite the operators of the hole on ASMM in terms of Hubbard operators,[37–39] i.e., $c_{\sigma} = X^{0\sigma}$, $c^{\dagger}_{\sigma} = X^{\sigma 0}$, $s_+ = X^{\uparrow\downarrow}$, $s_- = X^{\downarrow\uparrow}$, and $s_z = \frac{1}{2}(X^{\uparrow\uparrow} - X^{\downarrow\downarrow})$. Here the Hubbard operators $X^{\lambda\lambda'}$ are defined in terms of the hole states $|\lambda\rangle$ with $X^{\lambda\lambda'} \equiv |\lambda\rangle\langle\lambda'|$, satisfying the unity relation $\sum_{\lambda} X^{\lambda\lambda} = 1$. Similarly, by resolution of unity of large spin ($\sum_m Y^{mm} = 1$), we find

$$\begin{aligned} S_z &= \sum_{m=-S}^{S} m Y^{m,m}, \\ S_+ &= \sum_{m=-S}^{S} \sqrt{(S+m+1)(S-m)}\, Y^{m+1,m}, \\ S_- &= \sum_{m=-S}^{S} \sqrt{(S-m+1)(S+m)}\, Y^{m-1,m}. \end{aligned}$$

Here $Y^{mm'} \equiv |Sm\rangle\langle Sm'|$ and S is the length of large spin. One can verify these spin operators obey the basic commutation relation $[S_+, S_-] = 2S_z$. As a result, $H_{\rm cen}$ and $H_{\rm T}$ can be written as

$$\begin{aligned} H_{\rm cen} &= \epsilon_{\rm h}(X^{\uparrow\uparrow} + X^{\downarrow\downarrow}) + \frac{J}{2}\sum_{m=-S}^{S} m X^{\uparrow\uparrow} Y^{mm} \\ &\quad - \frac{J}{2}\sum_{m=-S}^{S} m X^{\downarrow\downarrow} Y^{mm}, \end{aligned} \tag{3}$$

$$H_{\rm T} = \sum_{k\alpha\sigma}(t_{k\alpha} c^{\dagger}_{k\alpha\sigma} X^{0\sigma} + {\rm H.c.}), \tag{4}$$

where in Eq. (3) we have neglected the transverse spin-flip terms due to $\gamma = 0$.

3. Hubbard operator Green function and transport calculation

In order to calculate transport properties of the model described above, we obtain some useful formulas based on the Hubbard operator Green function. Following derivation by Meir and Wingreen, one gets the usual expression for the current[40,41]

$$I = -\frac{2e}{h}\sum_{\sigma=\uparrow,\downarrow}\int {\rm d}\omega \Gamma_{\sigma}\left[f_{\rm L}(\omega) - f_{\rm R}(\omega)\right] {\rm Im}\, G^{\rm r}_{\sigma}(\omega), \tag{5}$$

where $G^{\rm r}_{\sigma}(\omega) \equiv \langle\langle c_{\sigma}|c^{\dagger}_{\sigma}\rangle\rangle^{\rm r}$ is the Fourier transform of the retarded Green function $G^{\rm r}_{\sigma}(t) = -{\rm i}\theta(t)\langle\{c_{\sigma}(t), c^{\dagger}_{\sigma}(0)\}\rangle$ and $f_{\alpha}(\omega) = [{\rm e}^{\beta(\omega-\mu_{\alpha})} + 1]^{-1}$ is the Fermi distribution function, with $\beta = 1/k_{\rm B}T$ and μ_{α} the chemical potential of lead α. In this work we consider the case of no spin polarization $\Gamma_{\uparrow} = \Gamma_{\downarrow}$ and symmetric coupling $\Gamma_{\rm L} = \Gamma_{\rm R} = 2\pi|t|^2\rho$, where $\rho = 1/2D$ is the DOS of leads for the square band approximation. The conductance G ($G \equiv {\rm d}I/{\rm d}V$) can be obtained from Eq. (5). Therefore the entire analysis falls on to derivations of retarded Green function $G^{\rm r}_{\sigma}(\omega)$. It is expressed as

$$G^{\rm r}_{\sigma}(\omega) = \langle\langle X^{0\sigma}|c^{\dagger}_{\sigma}\rangle\rangle^{\rm r} = \sum_{m}\langle\langle X^{0\sigma}Y^{mm}|c^{\dagger}_{\sigma}\rangle\rangle^{\rm r} \quad (\sigma = \uparrow, \downarrow)$$

in many-body representation, which can be determined by the equation of motion scheme. For example, the equation of motion of "mixed" Green function $\langle\langle X^{0\sigma}Y^{mm}|c^{\dagger}_{\sigma}\rangle\rangle^{\rm r}$ is

$$\begin{aligned} &\left(\omega - \epsilon_{\rm h} - \delta_{\sigma}\frac{J}{2}m\right)\langle\langle X^{0\sigma}Y^{mm}|c^{\dagger}_{\sigma}\rangle\rangle^{\rm r} \\ &= P_{0m} + P_{\sigma m} + \sum_{k\alpha} t^{*}_{k\alpha}\langle\langle X^{\bar{\sigma}\sigma}c_{k\alpha\bar{\sigma}}Y^{mm}|c^{\dagger}_{\sigma}\rangle\rangle^{\rm r} \\ &\quad + \sum_{k\alpha} t^{*}_{k\alpha}\langle\langle (X^{00} + X^{\sigma\sigma})c_{k\alpha\sigma}Y^{mm}|c^{\dagger}_{\sigma}\rangle\rangle^{\rm r}, \end{aligned} \tag{6}$$

where $\bar{\sigma}$ is opposite to σ and the averages $P_{\lambda m} \equiv \langle X^{\lambda\lambda}Y^{mm}\rangle$ denote the occupation probabilities of the many-body states. We first consider the second-order approximation[42] to close the equations of motion. In Eq. (6), the spin-flip term between the leads and the hole is neglected and the last term gives rise to $\sum_{k\alpha} t^{*}_{k\alpha}\langle\langle (X^{00} + X^{\sigma\sigma})c_{k\alpha\sigma}Y^{mm}|c^{\dagger}_{\sigma}\rangle\rangle^{\rm r} \approx \Sigma_0\langle\langle X^{0\sigma}Y^{mm}|c^{\dagger}_{\sigma}\rangle\rangle^{\rm r}$

(the self-energy $\Sigma_0 = \sum_{k\alpha} |t_{k\alpha}|^2 / (\omega - \epsilon_{k\alpha} + \mathrm{i}0^+)) = -\mathrm{i}\Gamma_\mathrm{L}$. So the Green function $\langle\langle X^{0\sigma} Y^{mm} | c_\sigma^\dagger \rangle\rangle^\mathrm{r}$ is obtained as

$$\langle\langle X^{0\sigma} Y^{mm} | c_\sigma^\dagger \rangle\rangle^\mathrm{r} = \frac{P_{0m} + P_{\sigma m}}{\omega - \epsilon_\mathrm{h} - \delta_\sigma \frac{J}{2} m - \Sigma_0}. \tag{7}$$

Thus the retarded Green function can be expressed as

$$G_\sigma^\mathrm{r}(\omega) = \sum_{m=-S}^{S} \frac{P_{0m} + P_{\sigma m}}{\omega - \epsilon_\mathrm{h} - \delta_\sigma \frac{J}{2} m - \Sigma_0}. \tag{8}$$

Next, for the Kondo regime, one needs to consider the lead-dot spin-flip process described by $\sum_{k\alpha} t_{k\alpha}^* \langle\langle X^{\bar{\sigma}\sigma} c_{k\alpha\bar{\sigma}} Y^{mm} | c_\sigma^\dagger \rangle\rangle^\mathrm{r}$ in Eq. (6). The equation of motion for the higher order Green function $\langle\langle X^{\bar{\sigma}\sigma} c_{k\alpha\bar{\sigma}} Y^{mm} | c_\sigma^\dagger \rangle\rangle^\mathrm{r}$ is

$$\begin{aligned} &(\omega - \epsilon_{k\alpha} - \delta_\sigma m J) \langle\langle X^{\bar{\sigma}\sigma} c_{k\alpha\bar{\sigma}} Y^{mm} | c_\sigma^\dagger \rangle\rangle^\mathrm{r} \\ &= \sum_{k'\alpha'} t_{k'\alpha'} \langle\langle X^{0\sigma} c_{k'\alpha'\bar{\sigma}}^\dagger c_{k\alpha\bar{\sigma}} Y^{mm} | c_\sigma^\dagger \rangle\rangle^\mathrm{r} \\ &\quad + \sum_{k'\alpha'} t_{k'\alpha'}^* \langle\langle X^{\bar{\sigma}0} c_{k'\alpha'\sigma} c_{k\alpha\bar{\sigma}} Y^{mm} | c_\sigma^\dagger \rangle\rangle^\mathrm{r}. \end{aligned} \tag{9}$$

Following Tolea and Bułka,[42] the higher order Green functions in the above equation are decoupled as

$$\begin{aligned} &\sum_{k'\alpha'} t_{k'\alpha'} \langle\langle X^{0\sigma} c_{k'\alpha'\bar{\sigma}}^\dagger c_{k\alpha\bar{\sigma}} Y^{mm} | c_\sigma^\dagger \rangle\rangle^\mathrm{r} \\ &\approx t_{k\alpha} f_\alpha(\epsilon_k) \langle\langle X^{0\sigma} Y^{mm} | c_\sigma^\dagger \rangle\rangle^\mathrm{r} \end{aligned}$$

with $f_\alpha(\epsilon_k) = \langle c_{k\alpha\sigma}^\dagger c_{k\alpha\sigma} \rangle$ the Fermi function and

$$\begin{aligned} &\sum_{k'\alpha'} t_{k'\alpha'}^* \langle\langle X^{\bar{\sigma}0} c_{k'\alpha'\sigma} c_{k\alpha\bar{\sigma}} Y^{mm} | c_\sigma^\dagger \rangle\rangle^\mathrm{r} \\ &\approx t_{k\alpha}^* \langle c_{k\alpha\sigma} c_{k\alpha\bar{\sigma}} \rangle \langle\langle X^{\bar{\sigma}0} Y^{mm} | c_\sigma^\dagger \rangle\rangle^\mathrm{r} = 0 \end{aligned}$$

by assuming that the operator pair of leads can be pulled out of the Green function and regarded as an average. Thus one can obtain from Eq. (9)

$$\sum_{k\alpha} t_{k\alpha}^* \langle\langle X^{\bar{\sigma}\sigma} c_{k\alpha\bar{\sigma}} Y^{mm} | c_\sigma^\dagger \rangle\rangle^\mathrm{r} = \Sigma_m^\sigma \langle\langle X^{0\sigma} Y^{mm} | c_\sigma^\dagger \rangle\rangle^\mathrm{r}, \tag{10}$$

where

$$\Sigma_m^\sigma = \sum_{k\alpha} |t_{k\alpha}|^2 f_\alpha(\epsilon_k) / (\omega - \epsilon_{k\alpha} - \delta_\sigma m J + \mathrm{i}0^+)$$

is the self-energy correction term under the third-order approximation. By substituting Eq. (10) into Eq. (6), the retarded Green function (8) is corrected as

$$G_\sigma^\mathrm{r}(\omega) = \sum_{m=-S}^{S} \frac{P_{0m} + P_{\sigma m}}{\omega - \epsilon_\mathrm{h} - \delta_\sigma \frac{J}{2} m - \Sigma_0 - \Sigma_m^\sigma}, \tag{11}$$

which can be used to discuss Kondo tunneling. The occupation probabilities $P_{\sigma m}$ of many-body states in Eqs. (8) and (11) can be calculated as

$$\begin{aligned} P_{\sigma m} &= \langle c_\sigma^\dagger X^{0\sigma} Y^{mm} \rangle = -\mathrm{i} \int \frac{\mathrm{d}\omega}{2\pi} G_{\sigma m}^<(\omega) \\ &= -\frac{1}{\pi} \int \mathrm{d}\omega \bar{f}(\omega) \mathrm{Im} \langle\langle X^{0\sigma} Y^{mm} | c_\sigma^\dagger \rangle\rangle^\mathrm{r}, \end{aligned} \tag{12}$$

where the lesser Green function $G_{\sigma m}^<(\omega)$ in the first line is defined as the Fourier transform of

$$G_{\sigma m}^<(t) \equiv \langle\langle X^{0\sigma}(t) Y^{mm}(t) | c_\sigma^\dagger(0) \rangle\rangle^< = \mathrm{i} \langle c_\sigma^\dagger(0) X^{0\sigma}(t) Y^{mm}(t) \rangle$$

and $\bar{f}(\omega) = (f_\mathrm{L}(\omega) + f_\mathrm{R}(\omega))/2$. In the last step of Eq. (12), the lesser Green function $G^< = G^\mathrm{r} \Sigma^< G^a$ is approximated by assuming that $\Sigma^< = \mathrm{i}(\Gamma_\mathrm{L} f_\mathrm{L} + \Gamma_\mathrm{R} f_\mathrm{R})$ by Ng's ansatz.[43] Substituting Eq. (7) into Eq. (12), one obtains a set of linear equations with respect to $P_{\sigma m}$

$$(C_{\sigma m} - 1) P_{\sigma m} + C_{\sigma m} P_{0m} = 0, \tag{13}$$

where

$$C_{\sigma m} = -\frac{1}{\pi} \int \mathrm{d}\omega \bar{f}(\omega) \mathrm{Im} \left[1 / \left(\omega - \epsilon_\mathrm{h} - \delta_\sigma \frac{J}{2} m - \Sigma \right) \right] \tag{14}$$

with $\Sigma = \Sigma_0$ for the sequential regime or $\Sigma_0 + \Sigma_m^\sigma$ for the Kondo regime. Here we would like to remark that we actually made a calculation by the master equation approach,[34] which is consistent with Eq. (13) in the sequential tunneling regime. Determining $P_{\uparrow m}$ and P_{0m} from Eq. (13) also require the use of the following relation

$$P_{0m} + P_{\uparrow m} + P_{\downarrow m} = \frac{1}{2S+1}, \tag{15}$$

which is due to the fact that the eigenvalue m of S_z is a good quantum number, i.e., there is no spin-flip mechanism between the hole and Mn spin. Thus the transport properties through the setup can be investigated based on the above formulas.

4. Numerical results and discussion

(i) Sequential tunneling regime

We now study numerically the occupation, conductance in the linear-response regime and nonlinear response regime. Sequential tunneling physics applies to the situation where the electrodes and center system is in the weak coupling limit, i.e., $\Gamma_\mathrm{L/R} \to 0$. In this limit, Eq. (14) gives rise to $C_{\sigma m} = \bar{f}(\epsilon_\mathrm{h} + \delta_\sigma \frac{J}{2} m)$, where we have used

$$-\int \frac{\mathrm{d}\omega}{\pi} \bar{f}(\omega) \mathrm{Im}[1/(\omega - a + \mathrm{i}\Gamma_\mathrm{L})] = \bar{f}(a)$$

for $\Gamma_\mathrm{L} \to 0$, and similarly the conductance is

$$\begin{aligned} G &= -(e^2 \Gamma_\mathrm{L}/h) \sum_\sigma \int \mathrm{d}\omega \, \mathrm{Im} G_\sigma^\mathrm{r}(\omega) \partial f_\mathrm{L} / \partial V(\omega) \\ &= (e^2 \Gamma_\mathrm{L}/h) \pi \sum_{m\sigma} (P_{0m} + P_{\sigma m}) \partial f_\mathrm{L} / \partial V(E_{\sigma m}), \end{aligned}$$

in which we bias the left electrode to $\mu_\mathrm{L} = V$ and leave $\mu_\mathrm{R} = 0$ and define $\partial f_\mathrm{L}/\partial V(\omega) = \beta \exp[\beta(\omega - V)]/[\exp[\beta(\omega - V)] + 1]^2$. For simplicity, we consider the case of $S = 1/2$ first. The center Hamiltonian H_cen has three branches of states: an empty sector $(N = 0)$ and two singly-occupied sectors $(N = 1)$, which include the parallel spin pair states (PS) and the antiparallel spin pair states (APS):

$$N = 0, \quad |0, \pm 1/2\rangle; \; E_0 = 0,$$

$$N = 1,\ \text{PS}: |\sigma, \pm 1/2\rangle;\ E_{\text{p}} = \epsilon_{\text{h}} + \frac{J}{4}, \qquad (16)$$
$$N = 1,\ \text{APS}: |\sigma, \mp 1/2\rangle;\ E_{\text{ap}} = \epsilon_{\text{h}} - \frac{J}{4},$$

where the upper (lower) sign applies for $\sigma = \uparrow (\downarrow)$. The occupation probabilities $P_{\lambda m}$ are determined by Eqs. (13) and (15), and they satisfy the relations $P_{0m} = P_{0-m}$ and $P_{\uparrow m} = P_{\downarrow -m}$ due to the symmetry of the Hamiltonian H_{cen}. Figure 1 shows the occupation probabilities and linear conductance as a function of ϵ_{h} for $S = 1/2$. The half-bandwidth D is taken as the energy unit in the sequential tunneling regime. In the region of $\epsilon_{\text{h}} > 0.3$, the occupation probabilities of the empty states approach $1/2$ and those of the other states approach zero, that is, there is no hole on the ASMM. With adjusting the gate voltage, the ϵ_{h} decreases gradually and the occupation probabilities of APS approach $1/2$ while those of the empty states vanish in $-0.3 < \epsilon_{\text{h}} < 0.3$. This means there is a hole occupying the APS. The corresponding linear conductance exhibits a resonant tunneling peak at $\epsilon_{\text{h}} = 0.3$ where APS energy level E_{ap} aligns with the Fermi energies (assumed to be zero) of two leads. This is a charge degeneracy point where the energy of the $N = 0$ states aligns with the energy of the $N = 1$ states and corresponding transitions are $\left|0, \pm\frac{1}{2}\right\rangle \Leftrightarrow \left|\bar{\sigma}, \pm\frac{1}{2}\right\rangle$ [Fig. 1(b)].

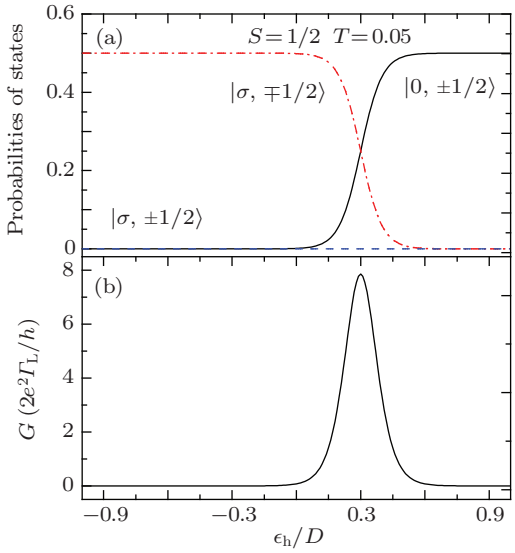


Fig. 1. (color online) Probabilities of states (a) and linear conductance (b) versus ϵ_{h} in the sequential tunneling regime for $S = 1/2$, $J = 1.2$, and $T = 0.05$. Energy unit is given here and in Figs. 2 and 3 in the half-bandwidth D. The upper (lower) sign applies for $\sigma = \uparrow (\downarrow)$.

For a CdTe QD doped with a single Mn^{+2} ion, i.e., the case of $S = 5/2$, a singly-occupied state level of the QD is split into six sublevels $E_{\sigma,m}$ ($E_{\uparrow,m} = E_{\downarrow,-m}$) with $m \in [-5/2,\ 5/2]$, due to the exchange interaction between the impurity spin S and a hole spin s. These spin pair states lead to transport properties different from the SMM and QD. As shown in Fig. 2, the linear conductance exhibits two three-peak structures. In fact, in the absence of a hole, the six projections S_z of Mn spin are degenerate ($E_{0,m} = 0$). But when a hole enters the QD, Mn spin and a hole spin can be coupled into PS $|\sigma, \pm|m|\rangle$ or APS $|\sigma, \mp|m|\rangle$, whose level scheme versus m is shown in the inset in Fig. 2. When the gate voltage sweeps the charge degeneracy region, the transitions between the $N = 0$ and $N = 1$ conserving S_z can only occur between $|0, \pm|m|\rangle$ and $|\bar{\sigma}, \pm|m|\rangle$. Thus the charge degeneracy points get tripled at $\epsilon_{\text{h}} = \frac{J}{2}|m|$, where the corresponding conductance exhibits three peaks [Fig. 2(b)]. However, we do not find the small, finite three-peak structure at $\epsilon_{\text{h}} = -\frac{J}{2}|m|$ at equilibrium.

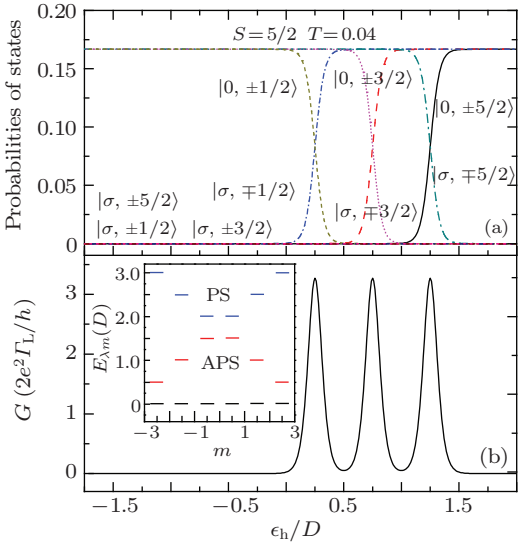


Fig. 2. (color online) Probabilities of various states (a) and linear conductance (b) versus ϵ_{h} in the sequential tunneling regime for $S = 5/2$, $J = 1$, and $T = 0.04$. Inset: the energy levels of eigenstates versus m with empty states (black bars), APS (red bars), and PS (blue bars). Parameters of inset are $\epsilon_{\text{h}} = 1.75, J = 1$. Results here by the nonequilibrium Green function method are consistent with the study of Contreras–Pulido and Aguado,[34] who found the three-peak structure in Fig. 2(a) of their work when $V = 0$.

When a bias voltage is applied to two electrodes, the sublevels enter the bias voltage window one by one with increasing bias voltage. Figure 3(a) presents the nonequilibrium occupation probabilities of all sublevels as a function of the bias voltage for $\epsilon_{\text{h}} = 2$, $J = 1$, and $T = 0.05$. For the bias voltage $V < 0.75$, the empty occupation dominates and $P_{0m} \to 1/6$. Whenever a new sublevel enters the bias voltage window, the occupation probability is reassigned to the sublevels in the bias voltage window. For example, in the region $0.75 < V < 1.25$, $P_{0,\pm\frac{5}{2}} = P_{\sigma,\bar{\sigma}\frac{5}{2}} \to \frac{1}{12}$ and $P_{0\pm\frac{3}{2}} = P_{0\pm\frac{1}{2}} \to 1/6$. The rest may be deduced by analogy. The property of the sequential tunneling current is shown in Fig. 3(b) and six steps in current (dashed line) and six peaks in differential conductance correspond to six sublevels. Whenever a sublevel comes into the bias voltage window the current appears as a step. The three higher peaks correspond to the resonant tunneling via three APS sublevels and the three lower peaks correspond to the resonant tunneling via three PS sublevels. This lower three-peak structure at nonequilibrium originates from the competition between APS and PS, see Fig. 3(a). Thus one can see the transport properties depend not only on the gate voltage or the bias voltage, but also on the quantum state of Mn spin.

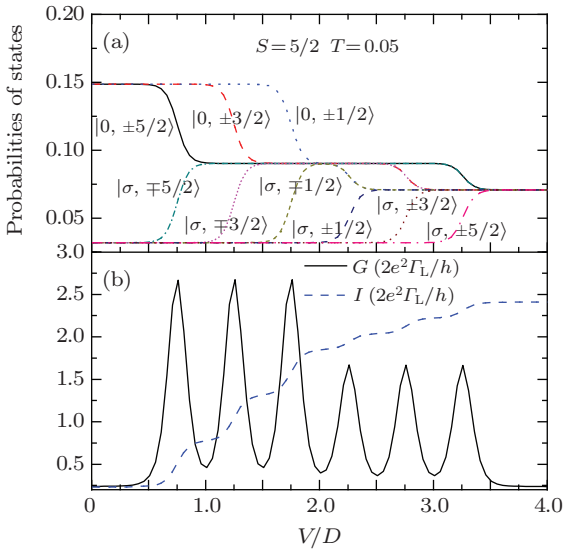


Fig. 3. (color online) (a) Nonequilibrium occupation probabilities of the states, (b) current and differential conductance as a function of the bias voltage for $S = 5/2$, $\epsilon_h = 2$, $J = 1$, and $T = 0.05$. In Fig. 3 we take $\mu_R = 0$ and bias the left lead to $\mu_L = V$.

(ii) Kondo tunneling regime

When the temperature is very low, in order to observe Kondo physics the higher-order approximation needs to be considered and the corresponding retarded Green function $G^r_\sigma(\omega)$ is given by Eq. (11). The DOS of the hole on the ASMM is calculated as $\rho_\sigma(\omega) = -(1/\pi)\mathrm{Im}\, G^r_\sigma(\omega)$. Figure 4 shows the DOS as a function of energy ω for $S = 1/2$, 1, $3/2$, 2, $5/2$, where we take $\epsilon_h = -2.5$ so that $2S+1$ sublevels are below the Fermi level. The total coupling $\Gamma = \Gamma_L + \Gamma_R$ is taken as the energy unit in the Kondo regime. It is found from Fig. 4 that $2S+1$ Kondo peaks in the DOS distribute symmetrically on both sides of the Fermi energy and are located at $\omega = Jm$, depending on the quantum state of the Mn spin. The Kondo peaks in the DOS originate from the many-body processes which occur in the low temperature regime and are related to the spin pair states. If a spin-down (or spin-up) hole occupies initially the APS level $E_{\downarrow|m|} = \epsilon_h - \frac{J}{2}|m|$, then it can tunnel into the Fermi level of a lead via the higher-order processes and simultaneously another spin-up (or spin-down) hole with energy $J|m|$ tunnels onto the PS level $E_{\uparrow|m|} = \epsilon_h + \frac{J}{2}|m|$. The coherent superposition of many such processes leads to the Kondo peaks in the DOS at the energy $\omega = J|m|$. In the same way one may explain the presence of the Kondo peaks at the energy $\omega = -J|m|$. We name this effect the spin-pair state Kondo effect. Strictly speaking, the Kondo effect here is the so-called underscreened Kondo effect because the hole spin does not screen the Mn spin in ASMM. The holes in the leads and on the sublevel form a spin-singlet state via higher-order processes, which leads to the Kondo effect depending on the parallel and antiparallel spin pair states.

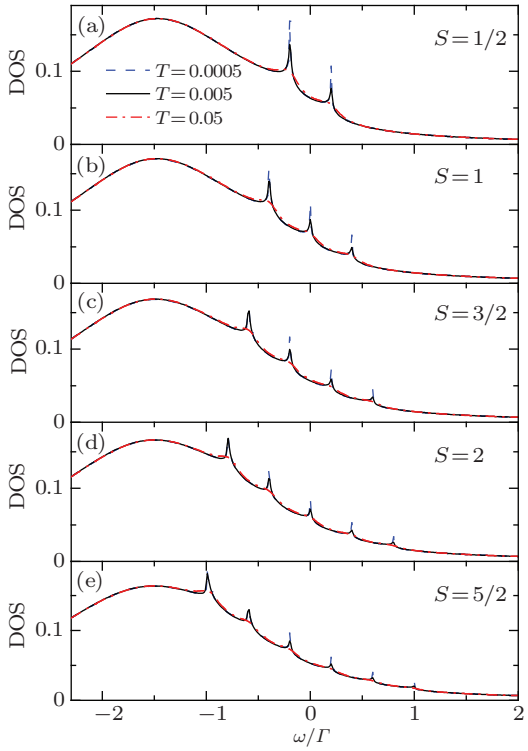


Fig. 4. (color online) Local density of states versus the energy ω at low temperature for ASMM spin $S = 1/2$, 1, $3/2$, 2, $5/2$. The parameters are chosen as $\epsilon_h = -2.5$, $J = 0.4$, and $D = 1000$ with the energy unit taken as the total coupling to the leads, i.e., $\Gamma = \Gamma_L + \Gamma_R = 1$.

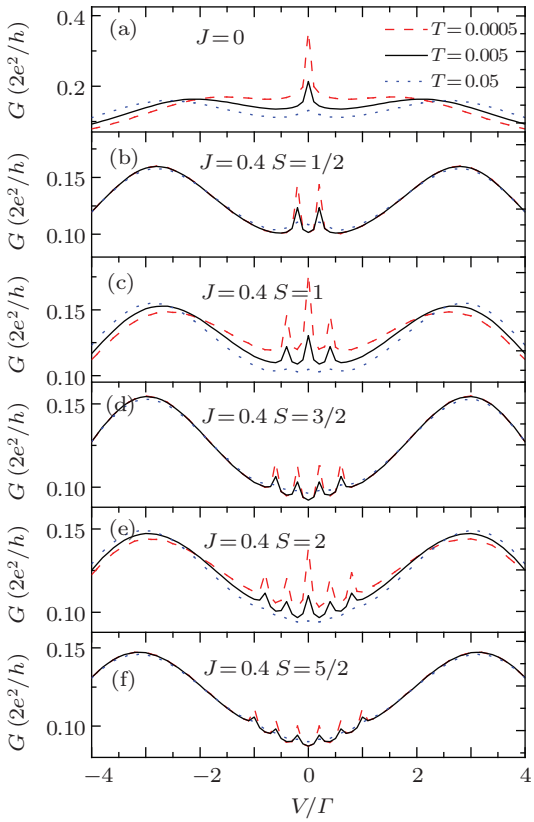


Fig. 5. (color online) Differential conductance versus the applied bias voltage for the exchange coupling (a) $J = 0$ and (b)–(f) $J = 0.4$. Other parameters are the same as those in Fig. 4. Energy is measured in Γ.

At very low temperature, the Kondo effect in the QD system typically presents as the increase of the tunneling conductance due to the resonance transmission via the Kondo peak in the DOS. In Fig. 5 we show the differential conductance as a function of the bias voltage applied symmetrically to two electrodes (i.e., $\mu_{\rm L} = V/2$, $\mu_{\rm R} = -V/2$). For $S = 0$ (or $J = 0$), there is merely one Kondo peak at the Fermi energy and this is the well-known QD result.[44] Two flat elastic resonant peaks are located at $V \sim 2\epsilon_{\rm h}$, as expected. For the case of $J \neq 0$, $(2S+1)$ Kondo peaks in differential conductance correspond to $(2S+1)$ peaks in the DOS, which attributes to $(2S+1)$ spin pair states formed by coupling of the impurity spin and a hole spin. With lowering the temperature, the Kondo peaks in conductance get higher. It is interesting that the dependence of two flat elastic resonant peaks on the temperature is related to the parity of the magnetic impurity spin.

5. Conclusion

In conclusion, we have investigated the transport properties of an artificial single-molecule magnet in the sequential and Kondo regimes. The transport setup considered is a minimal model based on CdTe QD doped with a single Mn^{+2} ion ($S = 5/2$), where the Mn–hole exchange interaction is strongly anisotropic so that the spin-flip of Mn spin is suppressed. The impurity spin S and a hole spin s entering the ASMM are coupled into the spin pair states with $(2S+1)$ sublevels. Correspondingly, in the sequential tunneling regime, $(2S+1)$ peaks occur in the differential conductance. Whenever a sublevel comes into the bias voltage window the current appears as a step and a peak is added in the differential conductance. However, with the PS entering the bias voltage window they begin to compete with the APS and the current steps and the corresponding differential conductance peaks get smaller. In the Kondo tunneling regime, $(2S+1)$ Kondo peaks occur in differential conductance due to transporting via $(2S+1)$ peaks in the DOS, which originates from the spin-singlet state formed by the holes in the leads and on the ASMM via the higher-order processes and is related to the parallel and antiparallel spin pair states.

References

[1] González G and Leuenberger M N 2007 *Phys. Rev. Lett.* **98** 256804
[2] Leggett A J, Chakravarty S, Dorsey A T, Fisher M P A, Garg A and Zwerger W 1987 *Rev. Mod. Phys.* **59** 1
[3] Heersche H B, de Groot Z, Folk J A, van der Zant H S J, Romeike C, Wegewijs M R, Zobbi L, Barreca D, Tondello E and Cornia A 2006 *Phys. Rev. Lett.* **96** 206801
[4] Romeike C, Wegewijs M R, Hofstetter W and Schoeller H 2006 *Phys. Rev. Lett.* **96** 196601
[5] Romeike C, Wegewijs M R, Hofstetter W and Schoeller H 2006 *Phys. Rev. Lett.* **97** 206601
[6] Jo M H, Grose J E, Baheti K, Deshmukh M M, Sokol J J, Rumberger E M, Hendrickson D N, Long J R, Park H and Ralph D C 2006 *Nano Lett.* **6** 2014
[7] Elste F and Timm C 2006 *Phys. Rev.* B **73** 235305
[8] González G, Leuenberger M N and Mucciolo E R 2008 *Phys. Rev.* B **78** 054445
[9] Elste F and Timm C 2010 *Phys. Rev.* B **81** 024421
[10] Misiorny M, Weymann I and Barnaś J 2011 *Phys. Rev. Lett.* **106** 126602
[11] Misiorny M and Barnaś J 2007 *Phys. Rev.* B **75** 134425
[12] Misiorny M and Barnaś J 2007 *Phys. Rev.* B **76** 054448
[13] Misiorny M and Barnaś J 2008 *Phys. Rev.* B **77** 172414
[14] Leuenberger M N and Mucciolo E R 2006 *Phys. Rev. Lett.* **97** 126601
[15] Candini A, Klyatskaya S, Ruben M, Wernsdorfer W and Affronte M 2011 *Nano Lett.* **11** 2634
[16] Peng J and Li S S 2012 *Chin. Phys. Lett.* **29** 047301
[17] Xue H B, Nie Y H, Li Z J and Liang J Q 2010 *J. Appl. Phys.* **108** 033707
[18] Xue H B, Nie Y H, Li Z J and Liang J Q 2011 *J. Appl. Phys.* **109** 083706
[19] Xue H B, Nie Y H, Li Z J and Liang J Q 2011 *Phys. Lett.* A **375** 716
[20] Chang B and Liang J Q 2011 *Chin. Phys.* B **20** 017307
[21] Fernández-Rossier J and Aguado R 2007 *Phys. Rev. Lett.* **98** 106805
[22] Xie Y, Duan S Q, Chu W D and Yang N 2010 *Chin. Phys.* B **19** 117304
[23] Xie Y, Duan S Q, Chu W D and Yang N 2010 *Chin. Phys.* B **19** 117302
[24] Zhong G H and Wang L M 2010 *Chin. Phys.* B **19** 107202
[25] Fang D K, Wu S Q, Zou C Y and Zhao G P 2012 *Chin. Phys. Lett.* **29** 037303
[26] Wang L, Zhao W, Hao Z B and Luo Y 2011 *Chin. Phys. Lett.* **28** 057301
[27] Sui B C, Fang L and Zhang C 2011 *Acta Phys. Sin.* **60** 077302 (in Chinese)
[28] Huang R, Song J, Guo Y Q, Wang X, Chen K J and Li W 2011 *Acta Phys. Sin.* **60** 027301 (in Chinese)
[29] Xie C M and Fan H Y 2011 *Chin. Phys.* B **20** 120303
[30] Li J, Wu S H, Zhang W W and Xi X Q 2011 *Chin. Phys.* B **20** 100308
[31] Xia J J and Nie Y H 2011 *Chin. Phys.* B **20** 097306
[32] Jia B Y, Yu Z Y, Liu Y M, Han L H, Yao W J, Feng H and Ye H 2011 *Chin. Phys.* B **20** 027302
[33] Wang Q, Liu J, Tang N and Zeng H S 2011 *Chin. Phys.* B **20** 020303
[34] Contreras-Pulido L D and Aguado R 2010 *Phys. Rev.* B **81** 161309
[35] Cronenwett S M, Oosterkamp T H and Kouwenhoven L P 1998 *Science* **281** 540
[36] Sasaki S, De Franceschi S, Elzerman J M, van der Wiel W G, Eto M, Tarucha S and Kouwenhoven L P 2000 *Nature* **405** 764
[37] Fransson Jonas 2010 *Non-Equilibrium Nano-Physics: A Many-Body Approach* (Dordrecht: Springer)
[38] Esposito M and Galperin M 2009 *Phys. Rev.* B **79** 205303
[39] Kostyrko T and Bułka B R 2005 *Phys. Rev.* B **71** 235306
[40] Meir Y and Wingreen N S 1992 *Phys. Rev. Lett.* **68** 2512
[41] Haug H J W and Jauho A P 2008 *Quantum Kinetics in Transport and Optics of Semiconductors* (Berlin: Springer)
[42] Tolea M and Bułka B R 2007 *Phys. Rev.* B **75** 125301
[43] Ng T K 1996 *Phys. Rev. Lett.* **76** 487
[44] Meir Y, Wingreen N S and Lee P A 1993 *Phys. Rev. Lett.* **70** 2601